

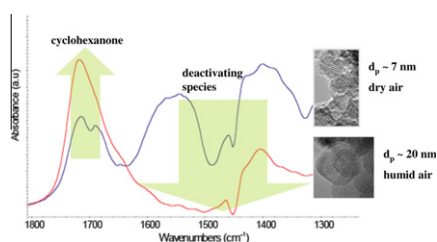


Contents

The effect of water on the performance of TiO₂ in photocatalytic selective alkane oxidation

pp 129–133

Joana T. Carneiro, Chieh-Chao Yang, Jacob A. Moulijn, Guido Mul*

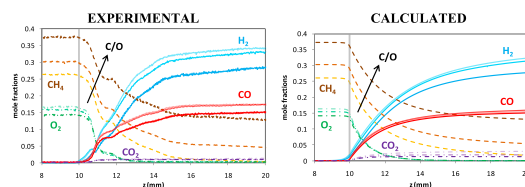


In-situ ATR-FTIR spectroscopy shows the absence of formation of deactivating species on anatase of high crystallinity when using humid air as oxidant in the liquid-phase photocatalytic oxidation of cyclohexane to cyclohexanone. The combination of beneficial surface chemical and opto-electronic properties of TiO₂ and humid air allows continuous cyclohexanone production.

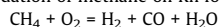
Modeling spatially resolved data of methane catalytic partial oxidation on Rh foam catalyst at different inlet compositions and flowrates

pp 134–148

D. Dalle Nogare*, N.J. Degenstein, R. Horn, P. Canu, L.D. Schmidt



Spatially resolved species and temperature profiles measured for a wide range of inlet stoichiometries and flowrates are compared with microkinetic numerical simulations to investigate the effect of transport phenomena on the catalytic partial oxidation of methane on Rh foam catalysts.

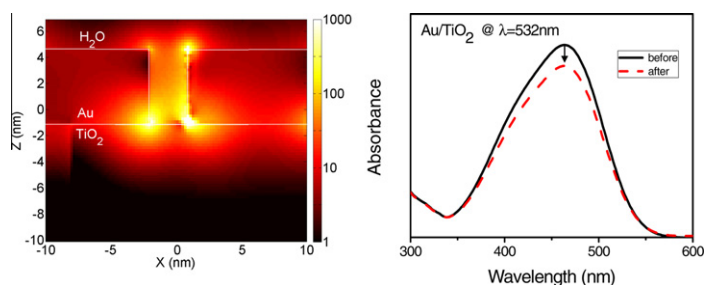


Experimental (left panel) and calculated (right panel) species profiles at a total inlet flowrate of $F = 5$ slpm and feed stoichiometries of $C/O = 0.8, 1.0$ and 1.3 (lighter to darker colors). CH₄, O₂ and H₂, CO, CO₂ mole fractions.

Plasmonic enhancement of photocatalytic decomposition of methyl orange under visible light

pp 149–153

Wenbo Hou, Zuwei Liu, Prathamesh Pavaskar, Wei Hsuan Hung, Stephen B. Cronin*

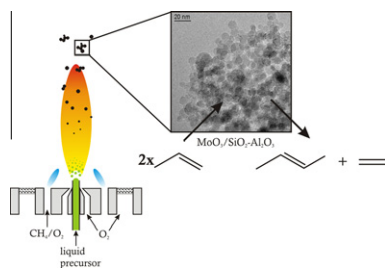


9-fold plasmonic enhancement in the photocatalytic decomposition rate of methyl orange was observed under visible illumination by integrating strongly plasmonic Au nanoparticles with strongly catalytic TiO₂. Finite-difference time-domain (FDTD) simulations indicate that the improvement in photocatalytic activity in the visible range can be attributed to the electric field enhancement in the interface of Au nanoparticles and TiO₂, rather than charge transfer.

Flame-made $\text{MoO}_3/\text{SiO}_2\text{-Al}_2\text{O}_3$ metathesis catalysts with highly dispersed and highly active molybdate species

pp 154–163

Damien P. Debecker*, Bjoern Schimmoeller*, Mariana Stoyanova, Claude Poleunis, Patrick Bertrand, Uwe Rodemerck, Eric M. Gaigneaux

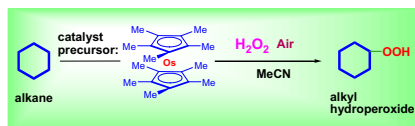


$\text{MoO}_3/\text{SiO}_2\text{-Al}_2\text{O}_3$ catalysts are produced in one step via flame spray pyrolysis. The solids produced consist in a silica-alumina matrix with Mo oxide on the surface. The MoO_x stabilized is highly dependant on the loading. The catalysts are tested in the metathesis of propene. Characterization shows that highly dispersed species are the most active. ToF-SIMS provides detailed insight on the degree of condensation of the MoO_x species at low loading.

Decamethylsmocene-catalyzed efficient oxidation of saturated and aromatic hydrocarbons and alcohols with hydrogen peroxide in the presence of pyridine

pp 164–172

Georgiy B. Shul'pin*, Marina V. Kirillova, Yuriy N. Kozlov, Lidia S. Shul'pina, Alexander R. Kudinov, Armando J.L. Pombeiro

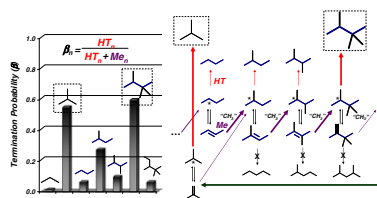


Decamethylsmocene, $(\text{Me}_5\text{C}_5)_2\text{Os}$ (1), is a pre-catalyst in a very efficient oxidation of alkanes with hydrogen peroxide in acetonitrile at 20–60 °C. Turnover numbers attain 51,000 in the case of cyclohexane (maximum turnover frequency was 6000 h^{-1}) and 3600 in the case of ethane.

Mechanistic details of acid-catalyzed reactions and their role in the selective synthesis of triptane and isobutane from dimethyl ether

pp 173–195

Dante A. Simonetti, John H. Ahn, Enrique Iglesia*

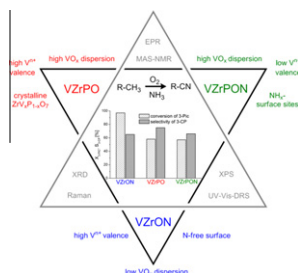


The selective homologation of C_1 species to isobutane and 2,2,3-trimethylbutane on solid acids reflects the relative stability of the carbenium ions involved in methylation and hydrogen transfer, the formation of isobutane via facile β -scission of chains larger than C_7 , and the substantial absence of isomerization or cracking for smaller chains. These reaction rates and chain termination probabilities were rigorously measured using mixtures of ^{13}C -dimethyl ether and ^{12}C -alkenes on H-BEA; their mechanistic interpretations are broadly applicable to chain growth and rearrangements of alkenes and alkoxydes via carbenium ion transition states.

Impact of phosphorus and nitrogen on structure and catalytic performance of VZrPON oxynitrides in the ammoxidation of 3-picoline

pp 196–207

C. Janke, M. Schneider, U. Bentrup, J. Radnik, A. Martin, G. Scholz, A. Brückner*

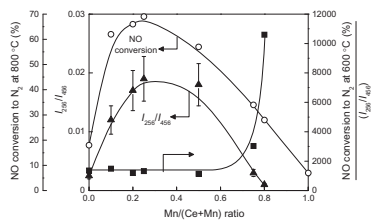


The catalytic performance of VZrON and novel P-containing VZrPON oxynitrides is compared in the ammoxidation of 3-picoline. Due to higher VO_x dispersion, lower V valence state and a pronounced formation of P–N instead of V–N bonds VZrPON catalysts are less active but slightly more selective.

Effect of Mn content on physical properties of CeO_x-MnO_y support and BaO-CeO_x-MnO_y catalysts for direct NO decomposition

pp 208–216

Won-Jong Hong, Shinji Iwamoto, Saburo Hosokawa, Kenji Wada, Hiroyoshi Kanai, Masashi Inoue*



Oxygen vacancies, whose concentration in the fluorite structure is assessed by the intensities of the Raman peak at 256 cm⁻¹, play an important role in direct NO decomposition on Ba-Ce-Mn catalysts.